# Evaluation of spectral similarity indices in unsupervised change detection approaches

Jeisson Fabián Ramos [a], Diego Renza [a] & Dora M. Ballesteros L. [a]

[a] Ingeniería en Telecomunicaciones, Universidad Militar Nueva Granada, Bogotá, Colombia. u1400856@unimilitar.edu.co, diego.renza@unimilitar.edu.co, dora.ballesteros@unimilitar.edu.co

**Abstract**
Unsupervised change detection (UCD) is a subject of Remote Sensing whose objective is to detect the differences between two multi-temporal images. In some cases, spectral similarity indices have been used as the comparison block in algorithms of UCD. The aim of this paper is to show in a quantitative way the performance of four spectral similarity indices in the correct identification of changes. Comparison is performed in terms of precision (overall accuracy and kappa index) over medium and high-resolution images (SPOT-5: Satellite Pour l'Observation de la Terre and Quickbird), with a reference obtained through a post-classification method (based on Support Vector Machines, SVM). The results show dependence on the automatic thresholding technique, as well as on the classes associated with the change.

*Keywords*: change detection; spectral indices; remote sensing; accuracy assessment.

# Evaluación de índices de similitud espectral en esquemas de detección de cambios no supervisados

**Resumen**
La detección de cambios de forma no-supervisada (UCD) es un área de teledetección, cuyo objetivo consiste en encontrar las diferencias entre dos imágenes multi-temporales. En algunos casos, los índices de similitud espectral son utilizados como bloque de comparación de UCD. El objetivo de este documento consiste en analizar de forma cuantitativa el desempeño de cuatro índices de similitud espectral en la correcta identificación de cambios. La evaluación se realiza en términos de la precisión (mediante la precisión global e índice kappa) utilizando imágenes de media y alta resolución (SPOT-5: Satélite Para la Observación de la Tierra y Quickbird), así como una imagen de cambio de referencia obtenida a través de un método de post-clasificación (basado en Máquinas de Soporte Vectorial, SVM). Los resultados obtenidos presentan dependencia con la técnica automática de umbralización, así como con las clases asociadas con el cambio.

*Palabras clave*: detección de cambios; índices espectrales; teledetección; evaluación de precisión.

## 1. Introduction

Recently, monitoring change of land surface characteristics is a topic of great importance whose objective is to detect the differences between two multi-temporal images. Research on change detection techniques have looked for new procedures to optimize some of the following characteristics related to the change analysis and its types: area and rate, spatial distribution, trajectories of land cover types, and accuracy evaluation of the results [1,2].

In a broad sense, a change detection project for remote sensing includes three main phases: pre-processing of the data, application of change detection approach, and accuracy assessment of the results [3,4]. The pre-processing phase can involve the following steps: (a) accurate register of multi-temporal images, (b) precise radiometric and atmospheric calibration or normalization between multi-temporal images, (c) having similar phenological stages between multi-temporal images, and (d) selecting the same spatial and spectral resolution [3].

Generally, change detection techniques can be classified into two groups, those that provide binary information (change/non-change) and those that provide information

transition between land cover changes [3,5]. The goal in the first group is to produce a binary change detection map in which the change areas are distinguished from unchanged areas. This is achieved by a direct comparison of the images; it is assumed that pixel values in change areas differ substantially between compared images, whereas this is not the case in unchanged areas. For this reason, the comparison can be performed directly on the spectral data. The result of the process is a difference image which can be analyzed to extract areas with significant changes. The most representative change/non-change methods are Image math (e.g. differencing, rationing or normalized indices differencing) and Transformations (e.g. Principal Components Analysis) [6]. Conversely, the second category relates to "from-to" detection. The aim of these methods is to generate a change detection map, where modified and transition classes in land use can be identified. In this case, the changes are detected and labeled through supervised classification schemes; therefore, post-classification comparison is a suitable kind of method to implement when sufficient training sample data are available [2,5].

In any case, there are four main components that allow to describe consistently a change detection technique. The first one relates to the input images, that usually involves the use of multi-temporal data sets, previously pre-processed [3]. The second one implies the definition of a unit of analysis, i.e. a kind of framework for the comparison over time; examples of analysis units can be image pixels, pixel kernel filter (moving window), systematic groups of pixels, image-objects, vector polygons, etc. [1,3]. As a third component, the comparison method allows to determine the presence of the change; some examples include image math, statistical approaches or post-classification schemes. Finally, a change map is obtained, which can be interpreted to obtain parameters such as the magnitude of the change (area, regions, etc.), or the transitions between land covers.

Regarding the analysis unit, the pixel is the simplest one, being an effective solution when its intensity is highly related to the land cover transitions of the multitemporal images under study [3]. This is an advantage of the image pixel as the unit of analysis, with regard to techniques such as kernel-based methods, where the computational cost can be an inconvenient in some cases [7]. On the other hand, an object is a group of pixels which includes context information and that typically involves the following steps: image segmentation; object extraction and comparison; and classification [1]. However, in methods that use image-object as the analysis unit, some external variations (e.g. illumination, viewing angle, phenology and atmospheric conditions) make the obtained object or segment highly variable, even with good pre-processing procedures [3].

Regarding the comparison method, in layer arithmetic operations, the level of change is obtained through the differences in image radiance of the input data; in addition, the input radiances can be previously converted to a most significant content using some indices, such as image ratios [3] or normalized differences (e.g. NDVI [8], NDWI [9], NDDI [9], etc.). In another context, the comparison is made by means of data reduction techniques that emphasize on the data with the highest variance, such as in the case of PCA-based (Principal Component Analysis) methods; in this case, the comparison method needs to be complemented with a framework to obtain change labels [1,2,3]. Finally, change detection magnitude and direction can be approached by analyzing feature vectors in the method known as Change Vector Analysis (CVA), which gives an intensity image and a direction image of change from the length and direction of the difference vector [10].

In some cases, the change detection approach is made in an unsupervised form. For instance, a clustering algorithm based on fuzzy c-means local information is proposed to CD in Synthetic aperture radar (SAR) images [11]. A recent approach proposes the use of PCA and k-means clustering to differentiate constructions in multitemporal images [2].

In order to make the comparison process and to obtain an intensity image of the change between two multitemporal images, some similarity metrics have been used, too. For instance, in [10], the ERGAS index (in French ''Erreur Relative Globale Adimensionnelle de Synthèse''), a metric to evaluate the spectral similarity in a fusion process, was proposed as the comparison method in an unsupervised change detection approach. The Spectral Angle Mapper (SAM) and the Spectral Correlation Mapper (SCM) were proposed in [12] to measure the similarity between two spectral feature vectors applied to change detection. Additionally, in [7], the angle between each multitemporal image and a reference vector measured by means of SAM metric was proposed as a solution for change detection in specific land covers.

The advantage of the application of similarity metrics lies in the reduction of the change detection problem to a 1-D problem [13]. Although kernel-based methods try to reduce the problem by running a linear algorithm in a higher dimensional feature space, its computational cost is higher than the direct comparison by means of a similarity metric. The simplicity of methods based on similarity metrics leads to ease the application and interpretation of the difference image, as with a simple threshold is sufficient to obtain the change map [1,13].

In the post-classification case, changes are identified through the comparison of the corresponding multitemporal thematic maps, and in consequence, it is a thematically rich technique [2], that can obtain changes in specific land covers; as an advantage, a radiometric normalization is not necessary, whereas the requirement of producing the whole thematic maps can be an inconvenient [5]. In complex scenarios for comparison purposes, the direct classification of multitemporal images is an alternative to get change information. Recently, Deep Learning techniques have been adopted in remote sensing to learn abstract representations of the input data [1], and applied to solving problems related to classification and change detection. Some examples include the use of Convolutional Neural Networks (CNN) trained with an unsupervised learning method seeking sparse feature representations [14], using fine-tuned CNN with linear SVM [15], superpixel-based feature extraction and difference representation learned by neural networks [1], Image classification by means of CNN [16], and building detection [17]. In any case, these methods require a considerable amount of labeled data [3,15,16].

In this sense, the objective of this paper is to make a comparison of four similarity indices applied to change detection. The selection of the indices has been conducted considering its aim, mainly oriented to detect spectral differences. According to

the above, the selected metrics are NDVI (Normalized Difference Vegetation Index), SAM (Spectral Angle Mapper), SCM (Spectral Correlation Mapper), and ERGAS indices, which are applied in an unsupervised form. Each method was applied between two multitemporal images, giving as result a difference image, and a change map after an automatic threshold is applied. For comparison purposes, a supervised post-classification method was implemented and its result was used to evaluate the overall accuracy and the kappa index of the results for the four unsupervised methods.

## 2. Material and methodology

### 2.1. Study area and datasets

Data for the study were obtained from both Community of Madrid, in Spain, and Indonesia. The zone in Spain includes a region between "San Fernando de Henares" and "Mejorada del Campo" at the Community of Madrid (Spain). The locator map is shown in Fig. 1(c). We used both SPOT-5 multispectral (MS) (2005) with SPOT-5 MS (2008) datasets related to urban, semi-urban and rural zones. For pre-processing, these Multi-temporal SPOT images were selected in anniversary dates to minimize sun angles and seasonal differences and they were registered using ENVI software. The images cover an area of 25 km$^2$ (500 × 500 pixels), and have a spatial resolution of 10 m. In this paper, the Green, Red and the Near-Infrared (NIR) bands of the SPOT-5 MS images were used for the change detection algorithms. The false color composition of the two multitemporal images is shown in Fig. 1. The upper left corner of the subset is placed at 40°25'24.7"N, 3°31'41.0"W.

The zone in Sumatra (Indonesia) is located on the northwestern tip of Sumatra Island, in the province of Aceh, Indonesia. The locator map is shown in Fig. 2(c). We used both Quickbird MS (April 2004) with Quickbird MS (January 2005) datasets relating to an area that was impacted by the December 26, 2004 tsunami, where many vegetation areas were washed out by it. For pre-processing, the Quickbird images were registered using ENVI software.
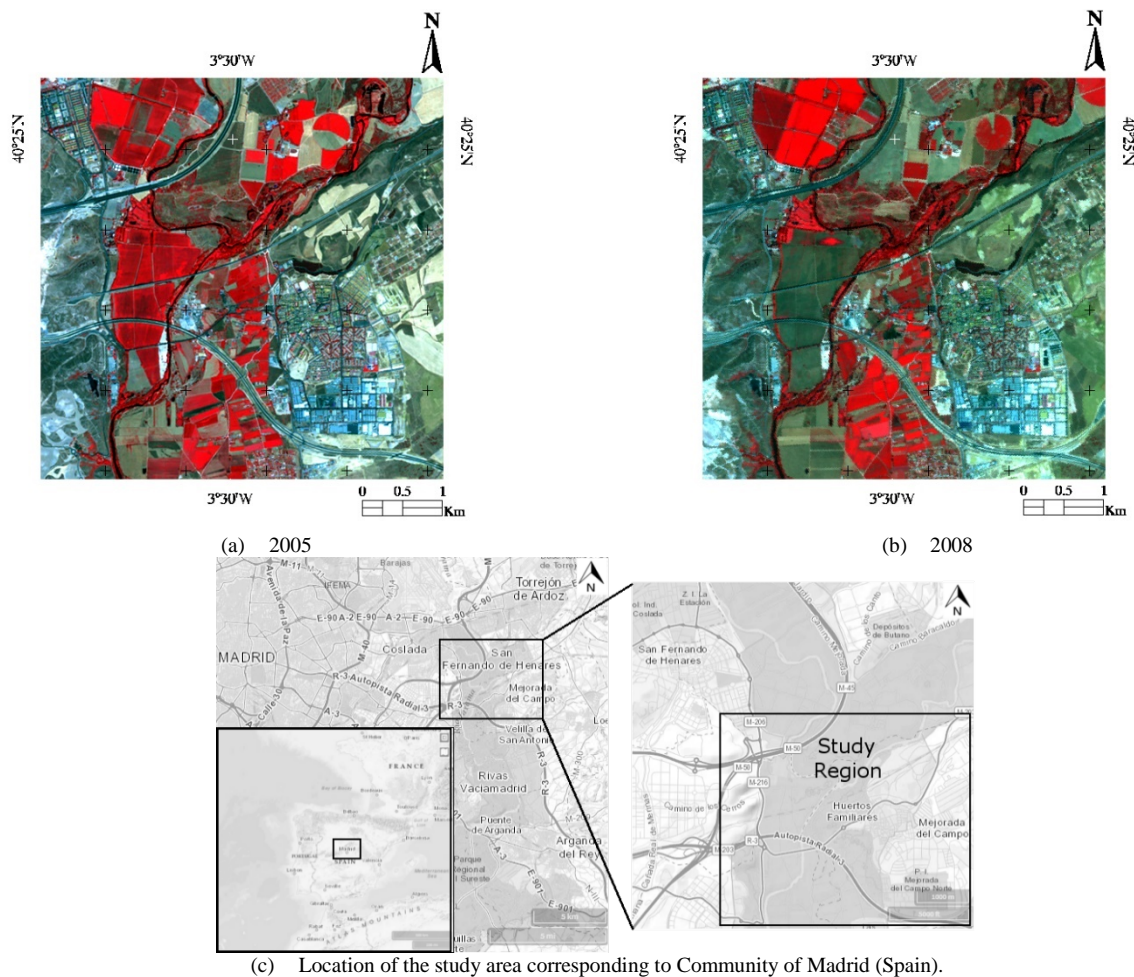


(a)   2005

(b)   2008

(c)   Location of the study area corresponding to Community of Madrid (Spain).

Figure 1. Multitemporal SPOT-5 Dataset. 25 km$^2$ (500 x 500 pixels), false color NIR, Red and Green composition. Community of Madrid (Spain). The upper left corner is placed at 5°18'14.7"N 95°12'04.4"E.
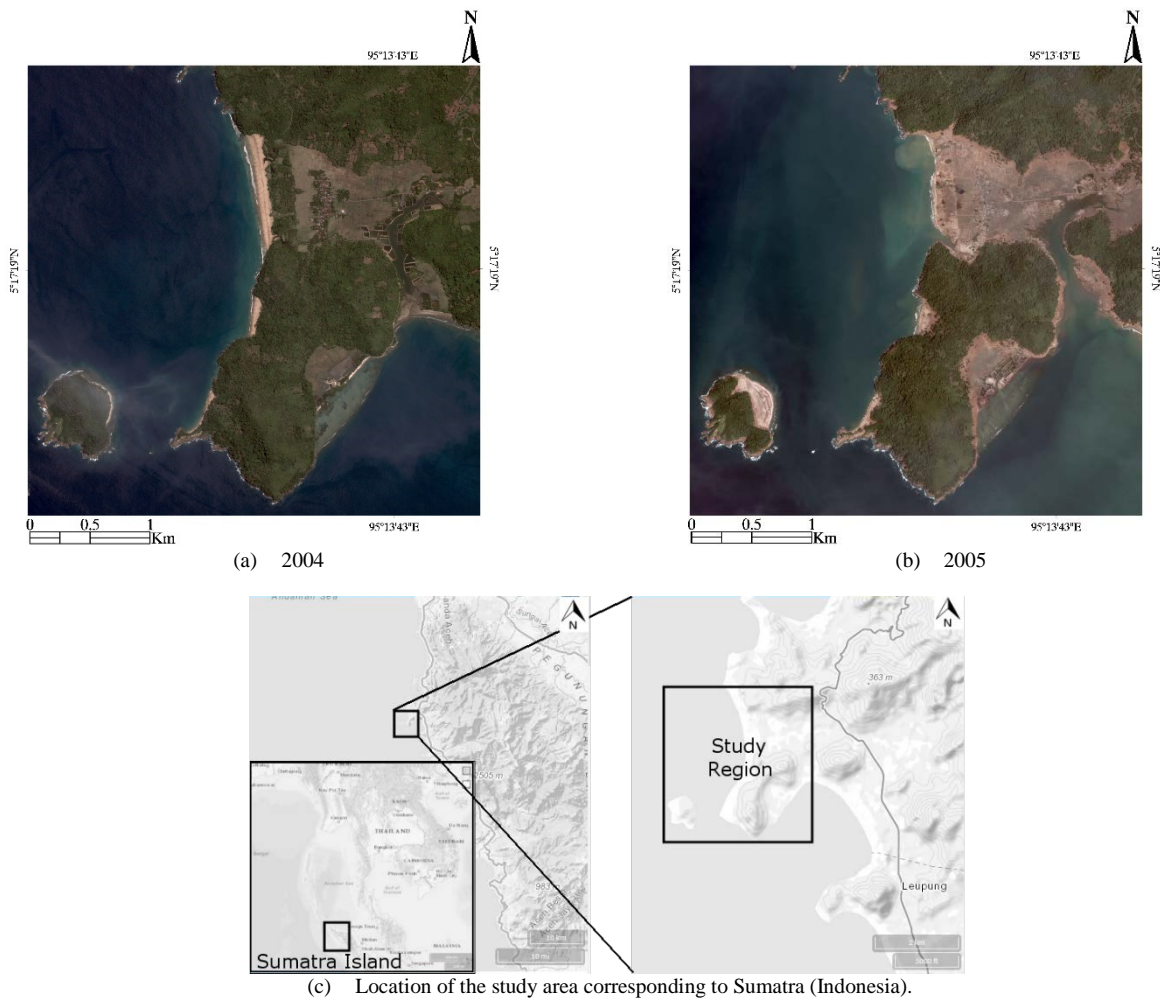Source: The authors.

(a) 2004


(b) 2005


(c)    Location of the study area corresponding to Sumatra (Indonesia).

Figure 2. Multitemporal Quickbird. ~14 km$^2$ (1500 x 1500 pixels), true color Red, Green and Blue composition. Sumatra (Indonesia). The upper left corner is placed at 40°25'24.7"N 3°31'41.0"W.
Source: The authors.

Also, the images cover an area of ~14 km$^2$ (1500 × 1500 pixels), and have a spatial resolution of 2.5 m. In the change detection algorithms, the four bands of the MS Quickbird images were used. The true color composite of the two multitemporal images is shown in Fig. 2. The upper left corner of the subset is placed at 5°18'14.7"N 95°12'04.4"E.

## 2.2. Spectral similarity indices

In order to compare the two multitemporal images, similarity metrics were selected. The aim is to evaluate the spectral differences between images, and obtain a simple difference image that reflects changes over time. The selected metrics include a conventionally used index to evaluate changes in vegetation: NDVI; this metric is a normalized difference of the reflectance in two spectral bands (red and NIR), so its application and computational cost is simple.

The following two proposed metrics correspond to indices used to evaluate the spectral quality of a fused image. The first is the ERGAS index [19], which was proposed to estimate the overall spectral error of a pan-sharpened image.

This index was modified as a spatial filter to evaluate changes [10]. In addition, the SAM index, originally proposed to evaluate the quality of a fused product, was recently used as a comparison index in a change detection approach [7].

The last selected metric is SCM. SCM is a spectral angular distance, just like SAM. These distances calculate the angle between each pixel of the images, considering each pixel as a vector in a space whose dimension is the number of bands of the image. Both metrics have been used for classification and clustering [12,19], as well as for change detection [7,12]. Their difference lies in the fact that SCM standardizes the data, centralizing it in the mean of the spectra of the two images. The mathematical functions behind the four spectral similarity indices are listed in Table 1.

## 2.3. Change detection methodology

The proposed change detection methodology includes an image registration phase, one supervised change detection approach, four unsupervised change detection approaches and an accuracy assessment stage (Fig. 3). The image

registration stage aligns the two MS images geometrically, to combine the pixels that represent the same objects.

The supervised stage includes a post-classification scheme, whose outcome will be used as the reference for evaluating the results of the unsupervised methods. The supervised method consists in classifying separately each MS image, defining some training areas for each class by an expert. The training areas are the inputs for the SVM (Support Vector Machine) classifier and its result is a new image including only the thematic classes. Finally, a logic comparison of the thematic classes of both images is applied and a reference binary image of change is obtained. The classification and post-classification change detection analysis were done in ENVI Software.

In the unsupervised change detection cases, each similarity metric of Table 1 is applied. This results in a gray scale image whose intensity reflects the intensity of change, whereby a thresholding algorithm is applied (Otsu's Algorithm). Finally, a binary image of change is obtained per each similarity metric. The NDVI method was done in ENVI software, whereas the remaining comparison metrics were implemented in MATLAB Software.

For accuracy assessment purposes, each binary image of change (the result of each similarity metric) is compared to the reference image (the result of the post-classification scheme) and an error matrix is obtained. The error matrix allows to calculate the overall accuracy and kappa index. These metrics were implemented in MATLAB software.

The flowchart of the study methodology is summarized in Fig. 3.

### 2.4. Accuracy assessment

The error matrix evaluation method is a valuable tool for assessing change detection results, therefore this will be the method used here. The error matrices are obtained by means of the comparison between the change map resulting from each one of the unsupervised methods and a reference, given by the change map obtained with the supervised method. The accuracy of the change detection methods is measured through Overall Accuracy ($OA$) and Kappa ($\kappa$) indices, where $OA$ is the ratio between pixels correctly classified and the total number of pixels, while $\kappa$ index measures statistically the concordance between the maps cited above [7].

According to the number of pixels correctly classified (CCp) (i.e. TP: true positives, and TN: true negatives), and to the number of pixels categorized erroneously (ICp) (i.e. FP: false positives, and FN: false negatives), the OA and the $\kappa$ indices are calculated as indicated in eq. (6)-(8).

$$OA = \frac{CC_p}{CC_p + IC_p} \tag{6}$$

$$\kappa = 1 - \frac{1 - OA}{1 - P_e} \tag{7}$$

Where,

$$P_e = \{P_1 P_2\} + \{(1 - P_1)(1 - P_2)\} \tag{8}$$

Table 1.
Mathematical functions of the used spectral similarity indices.

| Spectral similarity index | Mathematical function | |
|---|---|---|
| NDVI | $NDVI = \frac{(NIR - Red)}{(NIR + Red)}$ | (1) |
| | $NDVI_{DIFF} = |NDVI_{I^1} - NDVI_{I^2}|$ | (2) |

*NIR: Spectral reflectance in near-infrared band,*
*Red: Spectral reflectance in red band,*
*$I^i$ denotes Multitemporal image in time i*

| Local Ergas | $ERGAS(x,y) = 100 \sqrt{\frac{1}{N} \sum_{k=1}^{N} \left( \frac{f_k(x,y)}{g_k(x,y)} \right)^2}$ Where, $f_k(x,y) = \sqrt{\frac{1}{M} \sum_m \left( I_k^1(m) - I_k^2(m) \right)^2}$ $g(x,y) = \frac{1}{N} \sum_{k=1}^{N} \mu_k$ | (3) |
|---|---|---|

*x, y: denote spatial position (pixel position)*
*N denotes the number of spectral bands,*
*k denotes the index for each band*
*M, m denote window size and index in the spatial filter*
*$I^i_k$ denote Multitemporal band k in time i*

| SAM | $SAM_{CD} = COS^{-1} \left( \frac{\sum_{k=1}^{N} I_k^1 I_k^2}{\sqrt{\sum_{k=1}^{N} (I_k^1)^2 \sum_{k=1}^{N} (I_k^2)^2}} \right)$ | (4) |
|---|---|---|

*N denotes the number of spectral bands,*
*k denotes the index for each band*
*$I^i_k$ denote Multitemporal band k in time i*

| SCM | $SCM_{CD}$ $= COS^{-1} \left( \frac{\sum_{k=1}^{N} (I_k^1 - \bar{I}^1)(I_k^2 - \bar{I}^2)}{\sqrt{\sum_{k=1}^{N} (I_k^1 - \bar{I}^1)^2 \sum_{k=1}^{N} (I_k^2 - \bar{I}^2)^2}} \right)$ | (5) |
|---|---|---|

*N denotes the number of spectral bands,*
*k denotes the index for each band*
*$I^i_k$ denote Multitemporal band k in time i*
Source: The authors.

Table 2.
Land cover classification scheme and training sample size.

| Image | Class Name | Description | Training samples |
|---|---|---|---|
| SPOT | Vegetation | Fields where trees or crops grow | 2754 |
| | Water | Reservoirs, ponds, river, sea | 76 |
| | Buildings | Residential areas, urban service buildings, state highways. | 628 |
| | Bare soil 1 | Lands where vegetation is denuded or where the construction is underway | 586 |
| | Bare soil 2 | Lands where no vigorous vegetation grows | 1729 |
| Quickbird | Vegetation | Fields where trees or crops grow | 28186 |
| | Water | Reservoirs, ponds, river, sea | 105910 |
| | Bare soil 2 | Lands where no vigorous vegetation grows | 12718 |

Source: The authors.
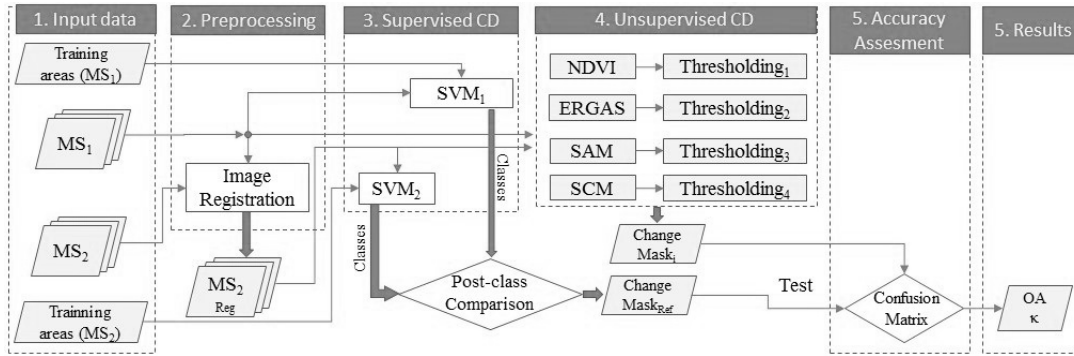
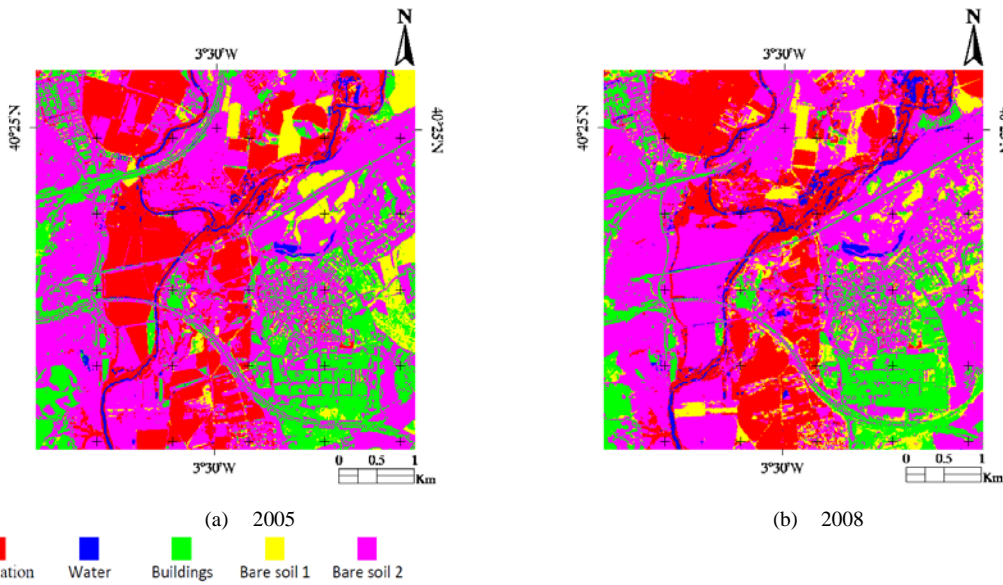Figure 3. Flowchart of the study methodology.
Source: The authors.



(a)    2005

(b)    2008

Vegetation    Water    Buildings    Bare soil 1    Bare soil 2

Figure 4. SPOT-5 classified images with the SVM supervised method.
Source: The authors.



(a)    2004
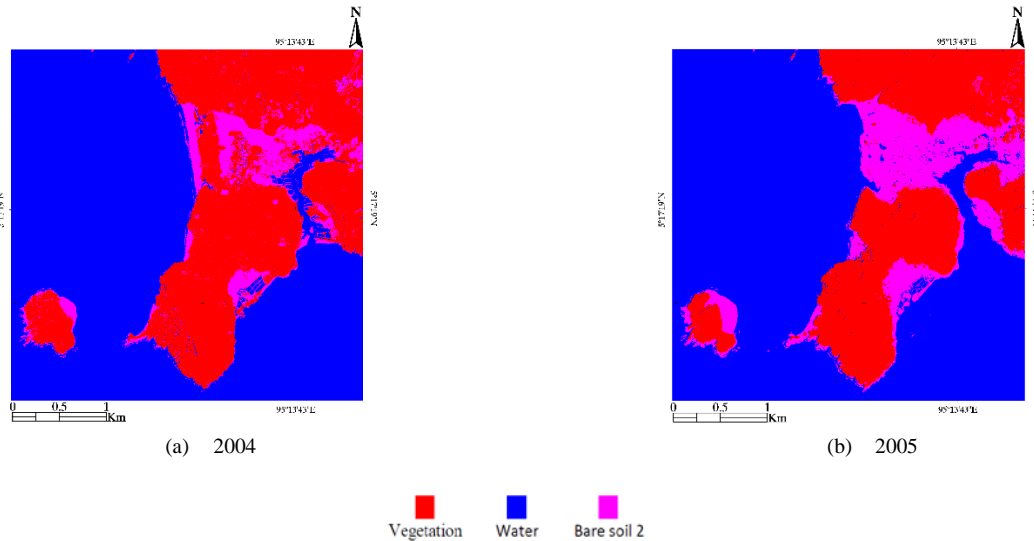
(b)    2005

Vegetation    Water    Bare soil 2

Figure 5. Quickbird classified images with the SVM supervised method.
Source: The authors.

Here $P_1$ represents the ratio between the number of samples identified as changed, and the total number of samples. $P_2$ represents the ratio between changed samples correctly identified, and the total number of samples.

## 3. Results

In this section, the results are shown in two parts: supervised method and unsupervised methods.

### 3.1. Supervised Method

For the supervised classification of the SPOT-5 images shown in Fig. 1, five thematic classes were defined in the training stage: vegetation, water, buildings, bare soil 1, and bare soil 2. See Table 2.

The SPOT-5 classified images are shown in Fig. 4. Then, the difference in each thematic class was evaluated and a unique binary image of change was obtained (Fig 6(a)). This image shows in white the areas where the supervised scheme has identified changes in all thematic classes, and it will be used as the reference image to evaluate unsupervised methods.

On the other hand, three thematic classes were defined to classify Quickbird images: vegetation, water, and bare soil 2 (Table 2). The classification results in the images shown in Fig. 5, and the respective comparison of their classes allows obtaining the change mask shown in Fig. 6(b). This binary image will be the reference to evaluate the unsupervised methods (Quickbird case).
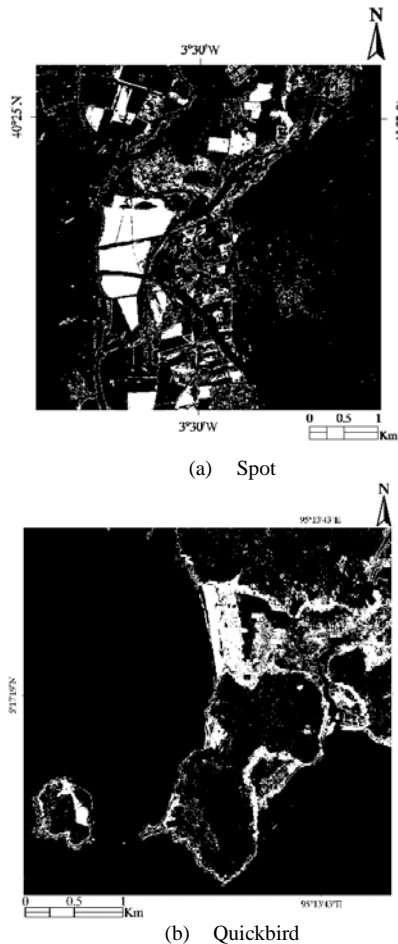
### 3.2. Unsupervised Methods

In the unsupervised methods, each metric defined in Table 1 was applied both for SPOT-5 and Quickbird MT images. The application of these metrics results in a difference image (grayscale) that was binarized using an automatic threshold given by the Otsu's method [1]. Figure 7 shows the SPOT-5 change maps obtained from each similarity metric. The images corresponding to NDVI, SAM, and SCM (Fig. 7(b-d)) show high correlation with Fig. 6(a); however, some differences are identified.

Figure 8 shows the change detection masks for the unsupervised case in Quickbird images. Here, the images corresponding to ERGAS, NDVI, and SAM (Fig. 8(a-c)) show some degree of similarity with Fig. 6(b).

For the evaluation of accuracy, it is important to bear in mind that it is possible to obtain the change mask for each class in the supervised method, while the unsupervised methods give a single image of change (integrating all the classes). For this reason, the results of the supervised method are integrated into a single image that is compared with the results of each unsupervised method.

### 3.3. Accuracy assessment

According to the comparison between the results of Fig. 6(a) and Fig. 7, and the comparison between the results of Fig. 6(b) and Fig. 8, error matrices were constructed. The coincidence in the identification of changed and unchanged zones in the reference image (supervised method) and in the



(a) Spot



(b) Quickbird

Figure 6. Change Maps obtained using the post-classification approach (SVM, supervised case). Change areas in white.
Source: The Authors.



(a) ERGAS
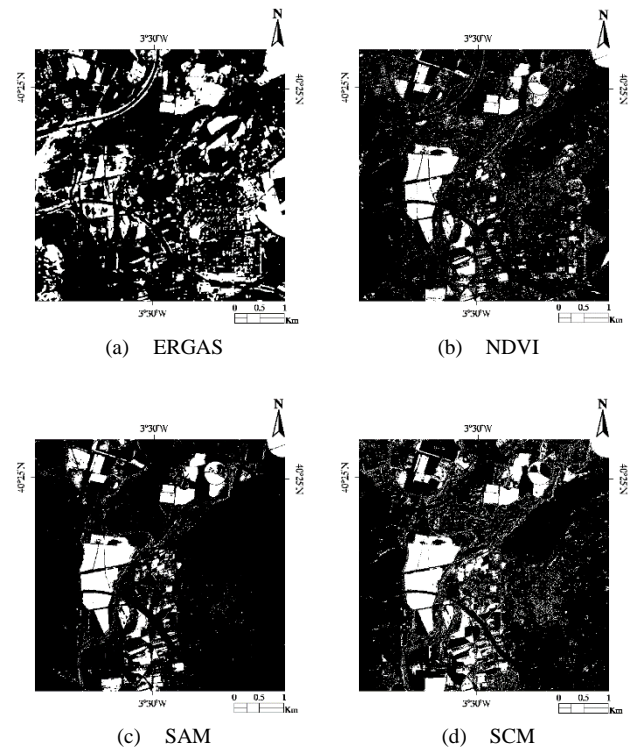


(b) NDVI



(c) SAM



(d) SCM

Figure 7. SPOT-5 change detection masks obtained through four similarity metrics and Otsu's thresholding algorithm (unsupervised case). Change areas in white.
Source: The authors.

(a)   ERGAS


(b)   NDVI


(c)   SAM


(d)   SCM

Figure 8. Quickbird change detection masks obtained through four similarity metrics and Otsu's thresholding algorithm (unsupervised case). Change areas in white.
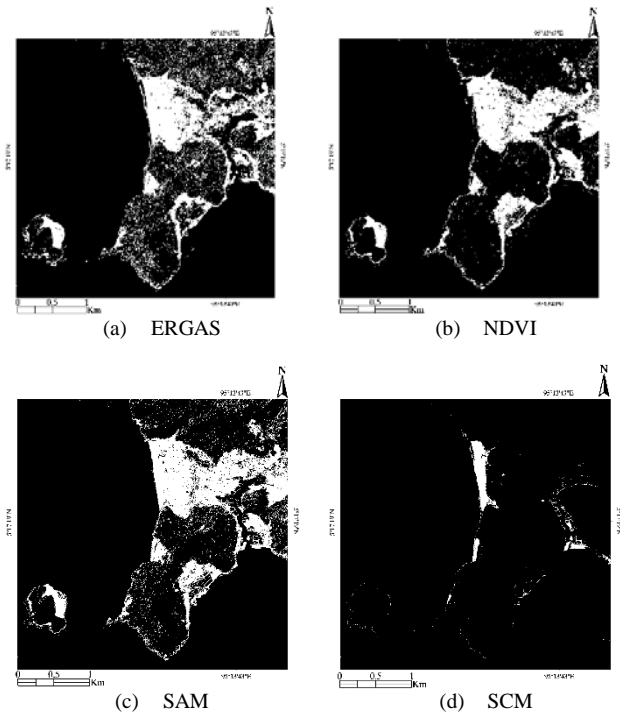Source: The authors.

Table 4.
Quickbird - Accuracy Assessment for ERGAS, NDVI, SAM and SCM, using Otsu's thresholding algorithm. Result: OA and κ. (C) Change (in Pixels) and (NC) Non-Change (in Pixels).

| Similarity index | | C | NC | Total | OA (%) | κ (%) |
|---|---|---|---|---|---|---|
| ERGAS | C | 195042 | 158237 | 353279 | 91,72 | 63,22 |
| | NC | 27977 | 1868744 | 1896721 | | |
| NDVI | C | 180659 | 113058 | 293717 | 93,09 | 66,10 |
| | NC | 42360 | 1913923 | 1956283 | | |
| SAM | C | 189844 | 130458 | 320302 | 92,73 | 65,09 |
| | NC | 33175 | 1896523 | 1929698 | | |
| SCM | C | 31274 | 5940 | 37214 | 91,21 | 21,82 |
| | NC | 191745 | 2021041 | 2212786 | | |
| Total | | 223019 | 2026981 | 2250000 | | |

Source: The authors.

The discussion about the above results will be performed in the next section.

## 4. Discussion

### 4.1. Spot images

The SPOT-5 images shown in Fig. 1 have a spatial resolution of 10 m (pixel size). Also, these images have a mixture of classes in the full scene, whereby five classes were defined in the post-classification method (supervised). According to the above, the unsupervised results for SPOT-5 images are lower than the Quickbird results.

The OA index shows a similar value (around 90%) for three approaches (NDVI, SAM and SCM), and the lowest value corresponds to ERGAS index. For kappa index, the highest value is obtained with SCM; however, the value for SAM is close to it. Again, the lowest value corresponds to ERGAS metric. The poorest results for ERGAS metric can be given for the high variability of classes in the studied SPOT-5 images and the behavior as a spatial filter (low pass) of this approach.

Visually, the change images shown in Fig. 7., highlight the main changes between the MT images, particularly for NDVI, SAM and SCM approaches. The main areas of change in these images are detected, whereas their differences are in small zones, whereby their differences can be given by the threshold level. The change image for ERGAS index does not show the trend in Fig. 6(a) and Fig. 7(b-d). This qualitative evaluation (visual inspection) corresponds with the results of quantitative evaluation (OA and κ index).

It is worth noting that the automatic thresholding technique can be an important player in the results of these approaches. However, these approaches were tested with maximum entropy thresholding scheme giving similar results.

### 4.2. Quickbird images

The Quickbird images shown in Fig. 2. have a spatial resolution of 2.5 m, and there are three classes that are easily identified. These features can lead to better results in Quickbird case than in SPOT-5 case. This is reflected in higher OA and κ values for Quickbird images as shown in

test images (unsupervised method) gives as a result changed pixels (C) and non-changed pixels (NC). TP is the pixels identified as C in both reference and test image. FP is the pixels identified as NC in the reference image and as C in the test image. FN is the pixels identified as C in reference image and as NC in the test image. Finally, TN is the pixels identified as NC, both in the reference and in the test image.

The error matrices for SPOT-5 results are shown in Table 3. For each similarity metric, Table 3 shows the number of pixels categorized as TP, FP, FN and TN. In any case, the sum of these values gives the total number of pixels in the SPOT-5 image, i.e. 250000 pixels (500 x 500). From these values, the OA and κ index are calculated and given.

In Quickbird case, Table 4 shows the error matrices for each similarity metric. Here, the sum of TP, FP, FN and TN is equal to 2250000 pixels, i.e. 1500 x 1500. Again, the OA and κ values are calculated and given as percentage values.

Table 3.
SPOT-5 - Accuracy assessment for ERGAS, NDVI, SAM and SCM, using Otsu's thresholding algorithm. Result: OA and κ. (C) Change (in Pixels) and (NC) Non-Change (in Pixels).

| Similarity index | | C | NC | Total | OA (%) | κ (%) |
|---|---|---|---|---|---|---|
| ERGAS | C | 11407 | 49101 | 60508 | 72,30 | 9,82 |
| | NC | 20140 | 169352 | 189492 | | |
| NDVI | C | 20688 | 15715 | 36403 | 89,37 | 54,78 |
| | NC | 10859 | 202738 | 213597 | | |
| SAM | C | 19853 | 10646 | 30499 | 91,06 | 58,90 |
| | NC | 11694 | 207807 | 219501 | | |
| SCM | C | 24544 | 18985 | 43529 | 89,60 | 59,45 |
| | NC | 7003 | 199468 | 206471 | | |
| Total | | 31547 | 218453 | 250000 | | |

Source: The authors.

Table 4. It is worth noting that most of the changes are related to vegetation class.

Regarding the number of classes, we must consider that having a smaller number of classes, their separability can be more precise in the post-classification method. This makes it possible to minimize the uncertainty in the results of the post-classification change detection method, which can finally affect the evaluation of unsupervised methods.

The Table 4 shows OA values higher than 90% for the four similarity metrics, and a κ index higher than 60% for three cases. Here the best results are obtained with ERGAS, NDVI and SAM approaches, being NDVI the best. The good performance in NDVI is based on the kind of changes shown in the Quickbird images, where some vegetation zones are changed to bare soil zones. Although SCM approach has a high OA value, its kappa index is very low, so the worst case is obtained with SCM. The main difference between SCM results and the other results is the number of true positive pixels, while the number of false negatives in SCM is high.

In the visual inspection, the ERGAS, NDVI and SAM image of change is similar to the reference image. In these three images, the main zone washed out by the tsunami (central zone) is bigger than the identified for the supervised approach. This leads to a high value of false negatives. Also, the ERGAS and SAM images show false positive pixels around all the peninsula. In SCM case, the zone identified as changed is very small, therefore its TP is lower ad its FN is higher than in other schemes. This behavior can be a consequence of a low threshold value given by the Otsu's method.

### 4.3. Recommendations

According to the above, for the application of similarity indexes in the detection of changes in remote sensing, the following recommendations and future work can be followed:

I. The selection of the similarity metric depends on the spatial resolution of the images. In low spatial resolution images, avoid the use of metrics that use spatial filtering (e.g. ERGAS).

II. The selection of similarity metrics depends on the type of classes present in the image. Some similarity indices are specifically geared to specific classes (e.g. NDVI). As future work it is possible to evaluate the performance of this type of metrics only in the class to which they are oriented.

III. When the area to be evaluated has a great variability of classes, together with a low spatial resolution (e.g. SPOT), the recommended methods are those based on spectral distances (e.g. SAM and SCM). On the contrary, in images with high spectral resolution and with low class variability, the use of spatial filtering-based metrics provided good results (e.g. ERGAS).

IV. Evaluate the impact of the thresholding method for each metric. Some thresholding methods may work better than others. As future work, it can be considered here to replace the thresholding by clustering (for example with the k-means algorithm).

### 5. Conclusion

This paper shows a comparison of four spectral similarity metrics applied to unsupervised change detection. The evaluation is done in terms of accuracy (OA and κ indices) and the results are obtained through the comparison against the results of a post-classification scheme based on SVM. The results have shown good performance for spectral angular distances, especially for SAM metric, whereas the SCM results can be dependent on the thresholding technique. The ERGAS index shows better results for high spatial resolution images (compared to medium resolution), since its behavior is like a spatial filter. Regarding NDVI, its results depend strongly on the percentage of vegetation changes in the multitemporal images evaluated. Another aspect to consider here is the variability of the classes in the image, where the precision in the image registration is a key factor, whereby the results in Quickbird image are better with regard to the results in SPOT-5 image.

According to the evaluation presented here, for images of low spectral resolution, the use of spectral distance based metrics is recommended, and the use of spatial filtering based metrics is recommended to avoid. For high-resolution images, both the distance-based and spectrum-based metrics showed good results. However, when the variability of classes is high, the spectral distance-based methods can have better results. As future work, it is recommended to consider clustering algorithms as an alternative to the thresholding phase and perform evaluation by classes in some similarity indexes.

### References

[1] Gong, M., Zhan, T., Zhang, P. and Miao, Q., Superpixel-based difference representation learning for change detection in multispectral remote sensing images. IEEE Transactions on Geoscience and Remote Sensing, 55(5), pp. 2658-2673, 2017. DOI: 10.1109/TGRS.2017.2650198

[2] Leichtle, T., Geiß, C., Wurm, M., Lakes, T. and Taubenböck, H., Unsupervised change detection in VHR remote sensing imagery–an object-based clustering approach in a dynamic urban environment. International Journal of Applied Earth Observation and Geoinformation, 54, pp. 15-27, 2017. DOI: 10.1016/j.jag.2016.08.010

[3] Tewkesbury, A.P., Comber, A.J., Tate, N.J., Lamb, A. and Fisher, P.F., A critical synthesis of remotely sensed optical image change detection techniques. Remote Sensing of Environment, 160, pp. 1-14, 2015. DOI: 10.1016/j.rse.2015.01.006

[4] Hussain, M., Chen, D., Cheng, A., Wei, H. and Stanley, D., Change detection from remotely sensed images: From pixel-based to object-based approaches. ISPRS Journal of Photogrammetry and Remote Sensing, 80, pp. 91-106, 2013. DOI: 10.1016/j.isprsjprs.2013.03.006

[5] Wu, C., Du, B., Cui, X. and Zhang, L., A post-classification change detection method based on iterative slow feature analysis and Bayesian soft fusion. Remote Sensing of Environment, 199, pp. 241-255, 2017. DOI: 10.1016/j.rse.2017.07.009

[6] Melgani, F., Moser, G. and Serpico, S.B., Unsupervised change-detection methods for remote-sensing images. Optical Engineering, 41(12), pp. 3288-3297, 2002. DOI: 10.1117/1.1518995

[7] Renza, D., Martinez, E., Molina, I. and Ballesteros-L., D.M., Unsupervised change detection in a particular vegetation land cover type using spectral angle mapper. Advances in Space Research, 59(8), pp. 2019-2031, 2017. DOI: 10.1016/j.asr.2017.01.027

[8] Coulter, L.L., Hope, A.S., Stow, D.A., Lippitt, C.D. and Lathrop, S.J., Time–space radiometric normalization of TM/ETM+ images for land

cover change detection. International Journal of Remote Sensing, 32(22), pp. 7539-7556, 2011. DOI: 10.1080/01431161.2010.524676

[9] Martínez, M., Martínez, M.E., Martínez, E. and Renza, D., Detection of changes in natural aquifer reservoirs based on the index of drought. IEEE Latin America Transactions, 15(11), pp. 2059-2053, 2017. DOI: 10.1109/TLA.2017.8070408

[10] Renza, D., Martinez, E. and Arquero, A., A new approach to change detection in multispectral images by means of ERGAS index. IEEE Geoscience and Remote Sensing Letters, 10(1), pp. 76-80, 2013.DOI: 10.1109/LGRS.2012.2193372

[11] Gong, M., Zhou, Z. and Ma, J., Change detection in synthetic aperture radar images based on image fusion and fuzzy clustering. IEEE Transactions on Image Processing, 21(4), pp. 2141-2151, 2012. DOI: 10.1109/TIP.2011.2170702

[12] Carvalho-Júnior, O.A., Guimarães, R.F., Gillespie, A.R., Silva, N.C., and Gomes, R.A., A new approach to change vector analysis using distance and similarity measures. Remote Sensing, 3(11), pp. 2473-2493, 2011. DOI: 10.3390/rs3112473

[13] Bovolo, F., Marchesi, S. and Bruzzone, L., A framework for automatic and unsupervised detection of multiple changes in multitemporal images. IEEE Transactions on Geoscience and Remote Sensing, 50(6), pp. 2196-2212, 2012. DOI: 10.1109/TGRS.2011.2171493

[14] Romero, A., Gatta, C. and Camps-Valls, G., Unsupervised deep feature extraction for remote sensing image classification. IEEE Transactions on Geoscience and Remote Sensing, 54(3), pp. 1349-1362, 2016. DOI: 10.1109/TGRS.2015.2478379

[15] Nogueira, K., Penatti, O.A. and dos Santos, J.A., Towards better exploiting convolutional neural networks for remote sensing scene classification. Pattern Recognition, 61, pp. 539-556, 2017. DOI: 10.1016/j.patcog.2016.07.001

[16] Sharma, A., Liu, X., Yang, X. and Shi, D., A patch-based convolutional neural network for remote sensing image classification. Neural Networks, 95, pp. 19-28, 2017. DOI: 10.1016/j.neunet.2017.07.017

[17] Vakalopoulou, M., Karantzalos, K., Komodakis, N. and Paragios, N., Building detection in very high resolution multispectral data with deep learning features. IEEE International Geoscience and Remote Sensing Symposium (IGARSS), 2015. pp. 1873-1876.

[18] Renza, D., Martinez, E. and Arquero, A., Quality assessment by region in spot images fused by means dual-tree complex wavelet transform. Advances in space research, 48(8), pp. 1377-1391, 2011.

[19] Hecker, C., Van der Meijde, M., van der Werff, H. and van der Meer, F.D., Assessing the influence of reference spectra on synthetic SAM classification results. IEEE Transactions on Geoscience and Remote Sensing, 46(12), pp. 4162-4172, 2008. DOI: 10.1109/TGRS.2008.2001035

**J.F. Ramos,** received the BSc. Eng in Telecommunication Engineering in 2017, from the Universidad Militar Nueva Granada (UMNG). Bogotá, Colombia. He is assistant researcher at the UMNG. His research interests include image and signal processing.
ORCID:0000-0002-1985-4335

**D. Renza,** received the MSc. degree in Telecommunications Engineering from the Universidad Nacional de Colombia in 2010, and the PhD. in Advanced Computing from the Universidad Politécnica de Madrid, Spain in 2015. He is currently working at Universidad Militar Nueva Granada, Colombia. His research interests include signal processing and remote sensing.
ORCID: 0000-0001-8073-3594

**D.M. Ballesteros L.,** received the MSc. degree in Electronic Engineering from University of Los Andes, Colombia, in 2004, and the PhD. in Electronic Engineering from the Universitat Politécnica de Cataluña, Spain, in 2013. She is currently working at Universidad Militar Nueva Granada, Colombia. Her research interests include signal processing and data hiding.
ORCID: 0000-0003-3864-818X

UNIVERSIDAD **NACIONAL** DE COLOMBIA

SEDE MEDELLÍN
FACULTAD DE MINAS

Área Curricular de Ingeniería
Eléctrica e Ingeniería de Control

Oferta de Posgrados

Maestría en Ingeniería - Ingeniería Eléctrica

Mayor información:

E-mail: ingelcontro_med@unal.edu.co
Teléfono: (57-4) 425 52 64